Int. J. Electrochem. Sci., 9 **(2014)** 6182 - 6190

International Journal of
ELECTROCHEMICAL
SCIENCE
www.electrochemsci.org

Coaxial $LiCoO_2$@Li_2MnO_3 Nanoribbon as a High Capacity Cathode for Lithium Ion Batteries

F.X. Wang[1], *S.Y. Xiao*[1], *Z. Chang*[1], *M.X. Li*[1], *Y.P. Wu* [1,*], *R. Holze*[2,*]

[1]New Energy and Materials Laboratory (NEML), Department of Chemistry & Shanghai Key Laboratory of Molecular Catalysis and Innovative Materials, Fudan University, Shanghai 200433, China
[2]Technische Universität Chemnitz, Institut für Chemie, AG Elektrochemie, D-09107 Chemnitz, Germany
[*]E-mail: wuyp@fudan.edu.cn; rudolf.holze@chemie.tu-chemnitz.de

Received: 18 July 2014 / *Accepted:* 8 August 2014 / *Published:* 25 August 2014

Coaxial $LiCoO_2$@Li_2MnO_3 nanoribbons prepared by a new method have been characterized with X-ray diffraction, field emission scanning electron and transmission electron microscopy. As cathode material for lithium ion batteries they deliver a high reversible capacity of 180 mAh g^{-1}, which is very stable without capacity fading during cycling in the range of 2.0 - 4.8 V. This is different from the traditional Li_2MnO_3 prepared via solid solution method.

Keywords: Lithium ion battery; cathode; Li_2MnO_3; coaxial; nanoribbons

1. INTRODUCTION

Lithium ion batteries are now the dominating storage device for portable electronic devices. To expand the use of lithium ion batteries, for instance as the onboard energy storage for electric vehicles (EVs) and other mobile applications, the specific energy density has to be increased further. Increasing cell voltage and capacity of their cathode (positive mass) [1-4] are necessary to meet this challenge. Li_2MnO_3, which can be rewritten as $Li[Li_{1/3}Mn_{2/3}]O_2$ with C2/m space group symmetry, is known to be an electrochemically inactive material because of the presence of Mn(IV) [5,6]. However, it can be converted into an cathode material electrochemically active at above 4.5 V by extracting Li and oxygen from the structure either by chemical or electrochemical means [7,8]. Actually, the specific capacity of Li_2MnO_3 could reach an ideal value of 459 mAh g^{-1} upon complete extraction of Li^+ [9]. This value is significantly higher than that of the current cathode materials of lithium ion batteries: $LiCoO_2$ or $LiNi_{1/3}Co_{1/3}Mn_{1/3}O_2$ (270 mAh g^{-1}) [10,11], $LiMn_2O_4$ (148 mAh g^{-1}) [1,12,13], and $LiFePO_4$ (170 mAh g^{-1})[14,15]. It is an induced electro-active material with a layered structure, opening the

channel for high voltage batteries with very high specific capacity. This makes Li_2MnO_3 an appealing candidate for the next generation cathode material for lithium ion batteries.

Recently, nanostructured materials have been studied extensively for energy-related applications [16,17]. It is well known, that nanosized particles can have shorter diffusion pathways for Li^+ ions, thus allowing fast Li^+ ions diffusion in the bulk of the electrode and towards the electrode/electrolyte interface. However, applications of single-phase nano-materials are limited due to their intrinsic material properties such as low conductivity, low mechanical stability and associated side reactions. To surpass the limitations associated with single phase nano-materials, various hybrid nanostructures have been proposed [18-20]. For hybrid nanostructured materials, strong synergetic effects can be achieved by integrating the individual components with all the desired functions of each component. Among them, coaxial architectures have attracted special attention [21-26]. For example, a type of nanodevice constructed from Cu@C coaxial nanocables was fabricated by using a focused-ion-beam (FIB) deposition technique [22]. Coaxially structured Ag/carbon hybrid electrodes were prepared as the anode for lithium ion micro-batteries, which show excellent electrochemical performance [24]. Coaxial carbon nanospheres/carbon nanotubes exhibit a good combination of high specific discharge capacity and volumetric capacity, good cycling stability and rate capability [26]. Here, we report on $LiCoO_2$@Li_2MnO_3 coaxial nanoribbons as a cathode material for lithium ion batteries. Interestingly, this novel composite shows high reversible capacity and excellent cycling behavior, which is competitive with those of solid solution materials (such as $0.5Li_2MnO_3$-$0.5LiMn_{0.5}Ni_{0.5}O_2$ [27], $LiNiPO_4$-coated $0.5Li_2MnO_3$-$0.5LiCoO_2$ [28], and $0.3Li_2MnO_3$-$0.7LiNi_{1/3}Co_{1/3}Mn_{1/3}$-$O_2$ [29]).

2. EXPERIMENTAL

Preparation of the Li_2MnO_3 and coaxial $LiCoO_2$@Li_2MnO_3 nanoribbons: In a typical procedure of preparing $Na_{0.44}MnO_2$ nanoribbons, 1.034 g $MnCO_3$ and 0.419 g Na_2CO_3 were mixed with 45.0 g NaCl ground homogeneously in a ball mill for 3 h. The mixture was annealed at 850 °C for 5 h in a furnace, and subsequently naturally cooled to room temperature. The resulting product was washed with distilled water and then dried at 100 °C in a drying oven. The synthesis of $Li_{0.44}MnO_2$ nanoribbons was achieved via $Na_{0.44}MnO_2$ nanoribbons followed by ion exchange to replace sodium by lithium. The sodium/lithium ion-exchange experiments were performed using a molten salt composed of a mixture of $LiNO_3$ (88 mol %) and LiCl (12 mol %) at 400 °C for 1 h in air. Then 0.426 g $Li_{0.44}MnO_2$ and 0.505 g $LiNO_3$ were mixed and heat-treated at 600 °C for 1 h to get Li_2MnO_3 nanoribbons. To prepare the coaxial $LiCoO_2$@Li_2MnO_3 nanoribbons, 4 mmol Li_2MnO_3, 1 mmol $LiCH_3COO_2 \cdot H_2O$ and 1 mmol $Co(CH_3COO)_2 \cdot 4H_2O$ were dissolved in 30 ml distilled water, finally the solution was added into a solution of 1 mmol citric acid dissolved in 10 ml distilled water under stirring. The mixture was aged at 80 °C for 12 h. After the gel became dry, the powders were ground in an alumina boat. The obtained powders were heated at 250 °C for 3 h, then heated at 650 °C for 4 h followed by cooling to room temperature. In all heat-treatment procedures the rising rate of temperature was 1 $^{\circ}C \cdot min^{-1}$. All chemicals were of analytical grade, and the aqueous solutions were prepared with distilled water.

Material characterization: X-ray diffraction (XRD) patterns were collected using a BrukerD4 X-ray diffractometer (Bruker, Germany) with Ni-filtered CuK_α radiation (40 kV, 40 mA). Scanning electron micrographs (SEM) were obtained with a Philip XL30 microscope (Philips, The Netherlands) operated at 25 kV. Field emission scanning electron micrographs (FESEM) were obtained with a FE-SEM-4800-1, and transmission electron micrographs (TEM) were acquired using a JEOL JEM-2010 transmission electron microscope (JEOL, Japan) operated at 200 kV. Samples were first dispersed in ethanol and then collected using carbon-film-covered copper grids for analysis.

Electrochemical measurements: The working electrode was prepared by coating the *N*-methyl-2-pyrrolidone (NMP)-based slurry containing the prepared Li_2MnO_3 (or $LiCoO_2@Li_2MnO_3$) nanoribbon, acetylene black and PVDF in a weight ratio of 8 : 1 : 1 on aluminum foil (thickness: 20 μm) using the doctor-blade technique. The coated foils were punched into circular pieces (d =15 mm) and dried at 120 °C for 12 h under vacuum. The mass loading of Li_2MnO_3 (or $FePO_4@Li_2MnO_3$) was around 24 mg cm^{-2}. Celgard 2730 membrane and LIB315 (a standard 1 $mol \cdot l^{-1}$ $LiPF_6$ solution in a 1:1:1 mixture of ethylene carbonate, dimethyl carbonate, and diethyl carbonate, Guotaihuarong Chemical Plant) were used as the separator and the electrolyte, respectively. All cells were assembled in an Ar-filled glove box. The cyclic voltammetry was obtained between 2.0 and 5.0 V at a scan rate of 0.1 mV s^{-1}. The cycling test was carried out by a Land tester (CT2001A) between 2.0 and 4.8 V (vs. Li^+/Li) at a current density of 10 mA g^{-1}.

3. RESULTS AND DISCUSSION

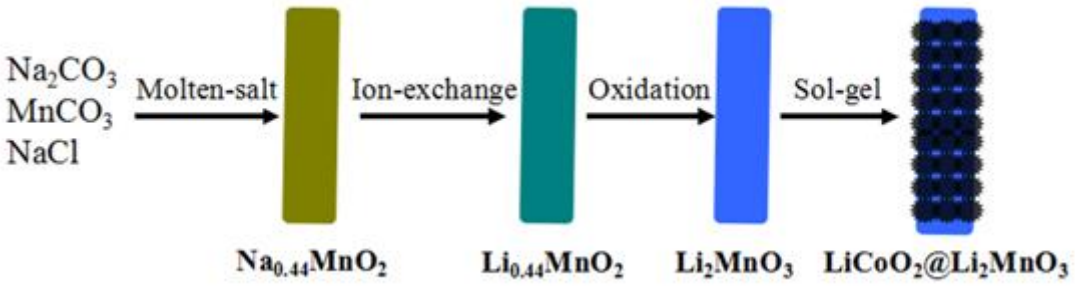

Scheme 1. The preparation process of the coaxial $LiCoO_2@Li_2MnO_3$ nanoribbons.

The preparation process of the coaxial $LiCoO_2@Li_2MnO_3$ nanoribbon is shown in Scheme 1. At first, $Na_{0.44}MnO_2$ nanoribbons were prepared by a simple molten salt method [30]. The crystallinity of the precursor template $Na_{0.44}MnO_2$ nanoribbons was measured by X-ray diffraction (XRD) (Fig. 1). The collected XRD pattern of the sample displays all the expected peaks from pure orthorhombic $Na_4Mn_9O_{18}$ (JCPDS No. 27-0750) [31].

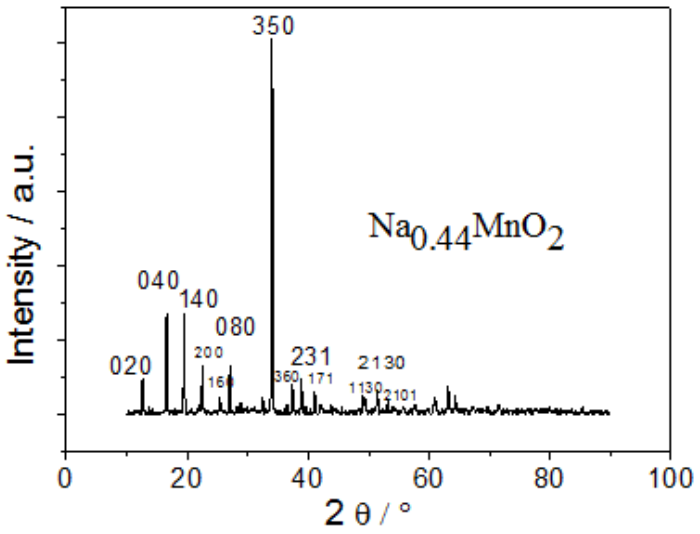

Figure 1. X-ray diffraction pattern of $Na_{0.44}MnO_2$

Then $Li_{0.44}MnO_2$ were obtained via $Na_{0.44}MnO_2$ nanoribbons as precursor followed by ion-exchange to replace Na^+ by Li^+. The sodium/lithium ion-exchange experiment was performed in a molten salt composed of a mixture of $LiNO_3$ (88 mol%) and LiCl (12 mol%) at 400 °C for 1 h in air. Then the Li_2MnO_3 was obtained by oxidation of $Li_{0.44}MnO_2$ nanoribbon. Finally, Li_2MnO_3 nanoribbon was decorated with $LiCoO_2$ nanoparticles using a sol-gel method.

The XRD diffraction patterns of the Li_2MnO_3 and the $LiCoO_2$@Li_2MnO_3 nanoribbons are shown in Fig. 2. Both samples show a layered structure with a C2/m space group, with alternating Li layers and transitional metal layers separated by oxygen layers. The superlattice peaks between 20 and 25° in the XRD, which are not observed in other layered materials, are due to the ordering of Li/Mn in the transitional metal layers [7]. However, it is noticeable that coexisting $LiCoO_2$ led to the reduction of the superlattice peaks derived from monoclinic Li_2MnO_3.

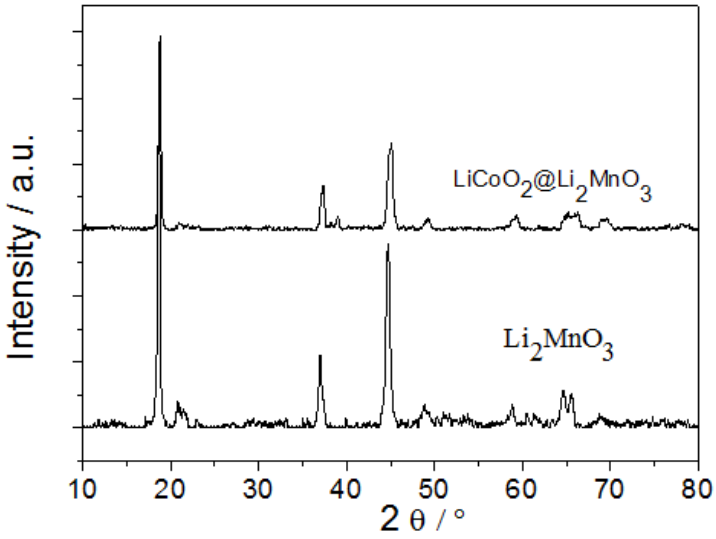

Figure 2. X-ray diffraction pattern of the as-prepared Li_2MnO_3 and $LiCoO_2$@Li_2MnO_3 nanoribbons.

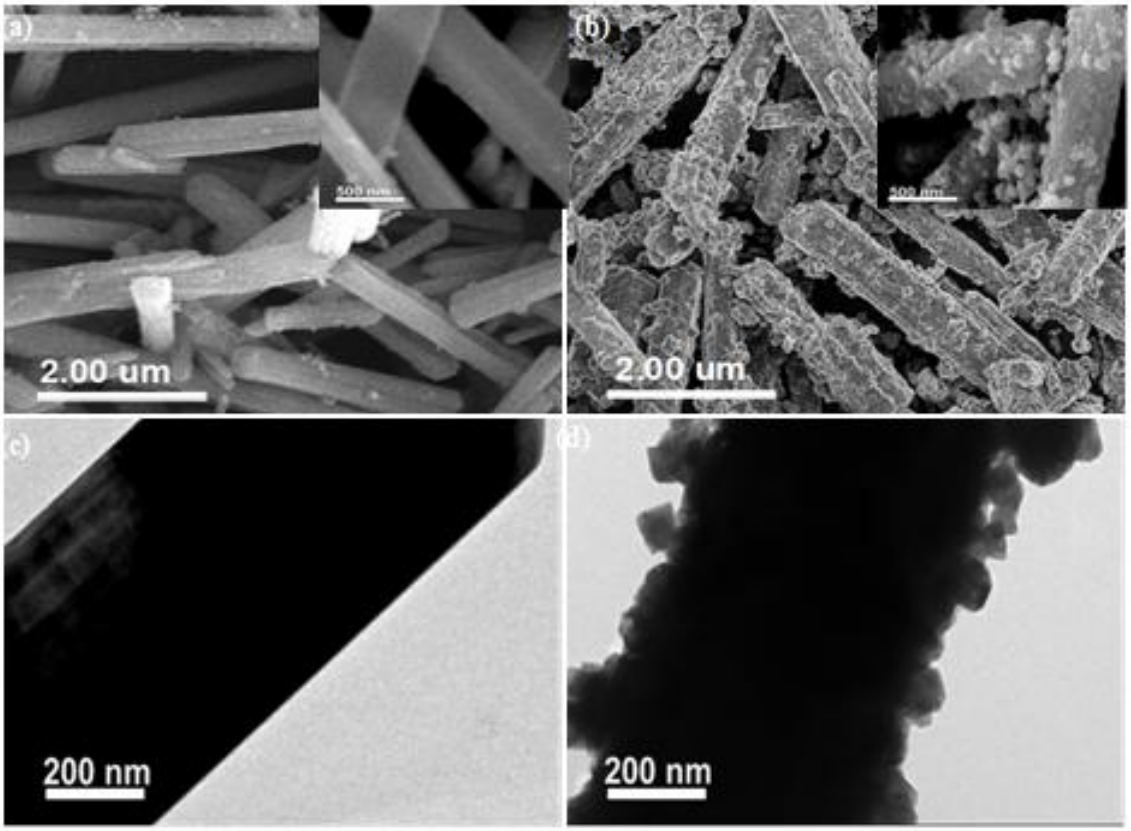

Figure 3. SEM and FESEM (insert) micrographs of the prepared (a) Li_2MnO_3 and (b) $LiCoO_2$@Li_2MnO_3 nanoribbons, and TEM micrographs of the prepared (c) Li_2MnO_3 and (d) $LiCoO_2$@Li_2MnO_3 nanoribbons.

The results were also observed in the solid solutions (Li_2MnO_3-$LiMO_2$) coated by other materials [28]. Fig. 3 shows the SEM and TEM micrographs of the prepared Li_2MnO_3 and $LiCoO_2$@Li_2MnO_3 nanoriboons. As shown in Fig. 2a, Li_2MnO_3 maintains the 1D morphology with diameters ranging from 200 to 500 nanometers. From the SEM and TEM micrographs of the $LiCoO_2$@Li_2MnO_3 nanoribbons, it could be seen that $LiCoO_2$ nanoparticles are uniformly loaded on the entire surfaces of each individual Li_2MnO_3 nanoribbon and the coaxial nanoribbon is maintained very well. This can be attributed to the fact, that $LiCoO_2$ nanoparticles tend to nucleate on the surface of the Li_2MnO_3 nanoribbon by minimizing the surface energy and then grow during the calcination process. The composition of the electrode is estimated by energy-dispersive X-ray spectroscopy (EDX) analyses from different parts of the sample, and the results reveal that the coaxial composite contains 22 wt% $LiCoO_2$. For comparison in Fig. 4 SEM micrographs of , $Na_{0.44}MnO_2$ and $Li_{0.44}MnO_2$ nanoribbons with diameters ranging from 200 nm to a few hundred nanometers and length up to several micrometers are displayed. Evidently, Li_2MnO_3 preserves the 1D morphology of $Na_{0.44}MnO_2$ nanoribbons although its surface is not so smooth as compared to that of $Na_{0.44}MnO_2$.

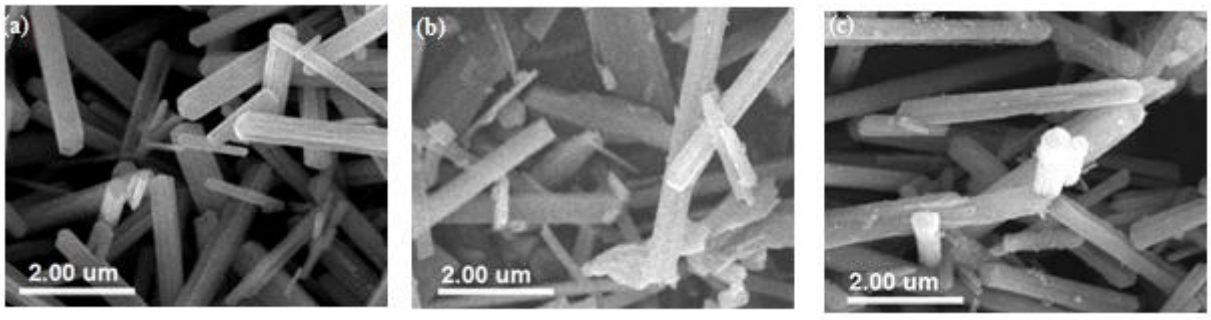

Figure 4. SEM micrographs of the prepared (a) $Na_{0.44}MnO_2$, (b) $Li_{0.44}MnO_2$ and (c) Li_2MnO_3.

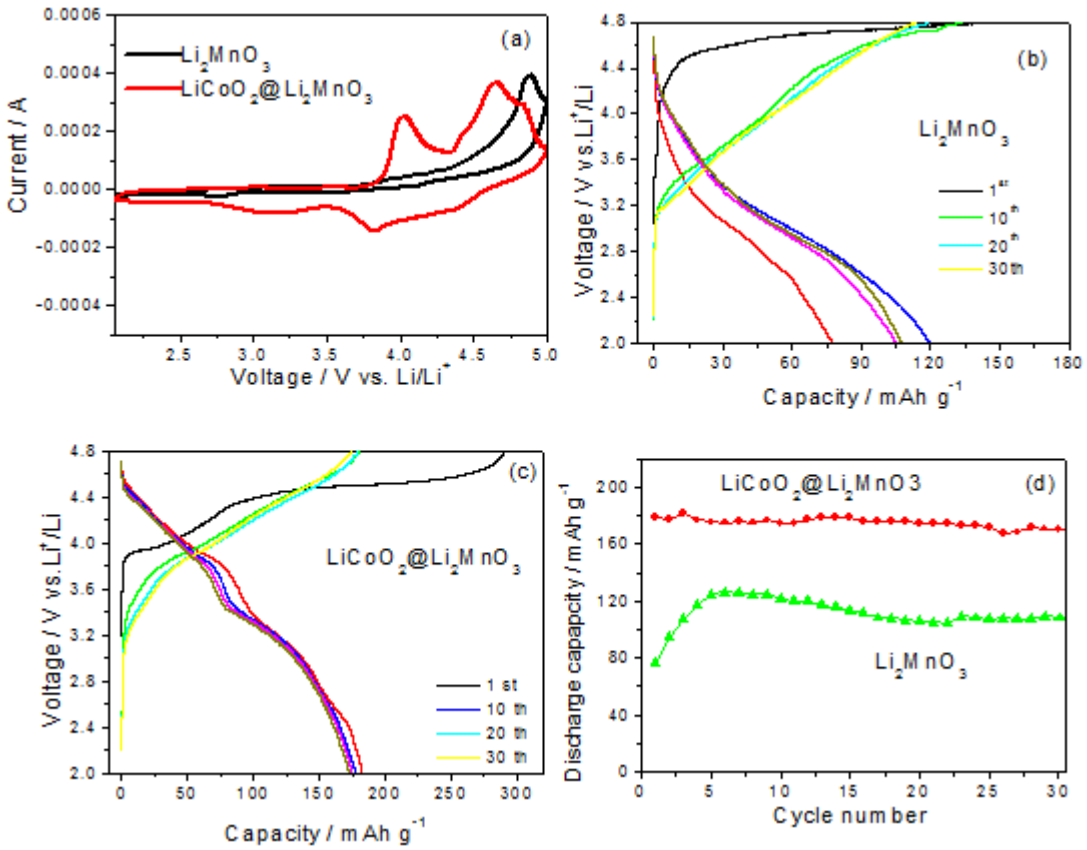

Figure 5. (a) Cyclic voltammograms of the Li_2MnO_3 and $LiCoO_2@Li_2MnO_3$ nanoribbons after the in tial charging process, the charge and discharge curves of (b) the Li_2MnO_3 nanoribbon and (c) the $LiCoO_2@Li_2MnO_3$ nanoribbon between 2.0 – 4.8 V, and (d) cycling behaviors of the Li_2MnO_3 and $LiCoO_2@Li_2MnO_3$ nanoribbons.

The electrochemical properties of the prepared $LiCoO_2@$ Li_2MnO_3 and Li_2MnO_3 nanoribbons are evaluated by cyclic voltammetry (CV), galvanostatic charge/discharge and cycling. From Fig. 5a it can be seen that there is one redox couple situated at 3.8/4.0 V vs. Li^+/Li for the $LiCoO_2@Li_2MnO_3$ coaxial nanoribbon, which is not observed in the curve for the Li_2MnO_3 nanoribbon after the first charging process. This is consistent with the plateaus attributed to the redox couple Co^{3+}/Co^{4+} in $LiCoO_2$ [10]. As shown in Fig. 5b, the Li_2MnO_3 nanoribbon exhibits initial charge and discharge

capacities of 142 mAh g^{-1} and 74 mAh g^{-1}, respectively. The lower initial charge capacity of Li_2MnO_3 is due to incomplete activation, i.e. removal of Li_2O from Li_2MnO_3 yielding active MnO_2, at this current density [32]. The capacity increases over several cycles. Such an interesting phenomenon is commonly observed for Li_2MnO_3, it is attributed to the activation process during the subsequent cycles. However, $LiCoO_2$@Li_2MnO_3 delivers a charge capacity as high as 270 mA h g^{-1} and a discharge capacity of 180 mA h g^{-1} (Fig. 5c). Two plateaus are present in the initial charge curve, which is consistent with the CV curve in Fig. 5a. The oxidation of Co^{3+} to Co^{4+} contributed to the former plateau [10]. The latter plateau starts at 4.5 V, which is generally known to be connected with the removal of oxygen from the cathode accompanied by diffusion of transition metal ions from surface to bulk where they occupy vacancies created by the removal of oxygen and lithium. [9, 33-37] The relatively low initial Coulombic efficiency for this composites is closely related to the irreversible lithium extraction/insertion from Li_2MnO_3. That is, lithium ions and O_2 were first removed from the core component Li_2MnO_3 during the activation process on the initial charging, which yields a component MnO_2 that can only accommodate one lithium ion per formula unit during discharging back to the rock-salt stoichiometry. Of course, not all the oxygen is lost as gas during the electrochemical process and some oxygen may react with the electrolyte [36,37]. Because of this, the as-prepared materials exhibit relative lower initial Coulombic efficiency compared to $LiCoO_2$, $LiNi_{1/3}Co_{1/3}Mn_{1/3}O_2$, $LiNi_{0.5}Mn_{0.5}O_2$ and other layered $LiMO_2$ materials [10,11,38]. Increasing the initial Coulombic efficiency and blocking the oxygen emission are still challenges for such composites to achieve the goal of practical application lithium ion battery cathode, which deserves further investigation in the future. Studies utilizing various coatings are currenly underway.

The cycling behavior is presented in Fig. 5d. Initially the discharge capacity of the Li_2MnO_3 nanoribbon increases due to transformation of the Li_2MnO_3 [27]. It reaches the highest discharge capacity, 125 mAh g^{-1}, in the sixth cycle, then decreases slowly. The main reason is the extraction of oxygen from the Li_2MnO_3 matrix during the activation process producing oxygen vacancies leading to structural destruction [39,40]. However, it has been observed that the $LiCoO_2$@Li_2MnO_3 nanoribbon shows no evident capacity fading at 180 mAh g^{-1} during the initial 30 cycles. The enhancement in the capacity and cycling behavior for the coaxial $LiCoO_2$@Li_2MnO_3 nanoribbon is attributed to the following reasons. Firstly, the $LiCoO_2$ nanoparticles on the surface of Li_2MnO_3, unlike electrochemically inactive oxides such as ZnO, AlF_3 and $AlPO_4$ on the surface of solid-solutions based on Li_2MnO_3, can provide available lithium ions for the insertion [28,41,42]. Secondly, the $LiCoO_2$ shell also contributes to reversible capacity from the CV and discharge and charge curves. Thirdly, the $LiCoO_2$ coating helps to suppress the structural destruction associated with the removal of oxygen and lithium ions [43]. However, further evidence and work including optimizing the $LiCoO_2$ content and increasing the initial Coulombic efficiency are needed.

4. CONCLUSION

In summary, a coaxial core-shell structured $LiCoO_2$@Li_2MnO_3 nanoribbon is prepared by using $Na_{0.44}MnO_2$ nanoribbons as the template. It delivers a high reversible capacity of 180 mAh g^{-1}

and excellent cycling performance. Its good electrochemical performance is ascribed to the core Li_2MnO_3 providing highly reversible capacity and the shell $LiCoO_2$ offering good protection. It presents a promise as a next generation cathode material for lithium ion batteries with high capacity and working

References

1. W. Tang, Y.Y. Hou, F.X. Wang, L.L. Liu,Y.P. Wu, K. Zhu, *Nano Lett*. 13 (2013) 2036.
2. N. Sharma, D. Yu,Y. Zhu, Y.P. Wu,V. K. Peterson, *Chem. Mater*. 25 (2013) 754.
3. Y. Shi, J.Z. Wang, S.L. Chou, D. Wexler, H.J. Li, K. Ozawa, H.K. Liu, Y.P. Wu, *Nano Lett*. 13 (2013) 4715.
4. Y.S. Zhu, S.Y. Xiao, Y. Shi, Y.Q. Yang, Y.Y. Hou and Y.P. Wu, Adv. *Energy Mater.* 4 (2014) 1300647.
5. Y. Paik, C.P. Grey, C.S. Johnson, J.S. Kim and M.M. Thackeray, *Chem. Mater.* 14 (2002) 5109.
6. A. D. Robertson and P. G. Bruce, *Chem. Commun.* (2002) 2790.
7. G. Singh, R. Thomas, A. Kumar and R. S. Katiyar, *J. Electrochem. Soc.* 159 (2012) A410.
8. J.R. Croy, S.H. Kang, M. Balasubramanian and M.M. Thackeray, *Electrochem. Commun.* 13 (2011) 1063.
9. Y. Okamoto, *J. Electrochem. Soc.* 159 (2012) A152.
10. X. Wang, Q. Qu, Y. Hou, F. Wang and Y. Wu, *Chem. Commun.* 49 (2013) 6179.
11. F. Wang, S. Xiao, Z. Chang, Y. Yang and Y. Wu, *Chem. Commun.* 49 (2013) 9209.
12. F.X. Wang, S.Y. Xiao, X.W. Gao, Y.S. Zhu, H.P. Zhang, Y.P. Wu and R. Holze, *J. Power Sources* 242 (2013) 560.
13. F.X. Wang, S.Y. Xiao, Y.S. Zhu, Z. Chang, C.L. Hu,Y.P. Wu and R. Holze, *J. Power Sources* 246 (2014) 19.
14. Y. Shi, S.L. Chou, J.Z. Wang, D. Wexler, H. J. Li, H.K. Liu and Y. Wu, *J. Mater. Chem.* 22 (2012) 16465.
15. Y. Hou, X. Wang, Y. Zhu, C. Hu, Z. Chang, Y. Wu and R. Holze, *J. Mater. Chem. A* 1 (2013) 14713.
16. Q. Zhang, E. Uchaker, S. L. Candelaria and G. Cao, *Chem. Soc. Rev.* 42 (2013) 3127.
17. J.N. Tiwari, R.N. Tiwari and K.S. Kim, Prog. Mater. Sci. 57 (2012) 724.
18. G. Yu, L. Hu, M. Vosgueritchian, H. Wang, X. Xie, J.R. McDonough, X. Cui, Y. Cui and Z. Bao, *Nano Lett.* 11 (2011) 2905.
19. M. Sathiya, A.S. Prakash, K. Ramesha, J.M. Tarascon and A.K. Shukla, *J. Am. Chem. Soc.* 133 (2011) 16291.
20. Q. Qu, Y. Zhu, X. Gao and Y.P. Wu, *Adv. Energy Mater.* 2 (2012) 950.
21. P. Wu, N. Du, H. Zhang, J. Yu and D. Yang, *J. Phys. Chem. C* 114 (2010) 22535.
22. W. Xu, Y. Zhang, Z. Guo, X. Chen, J. Liu, X. Huang and S.H. Yu, *Small* 8 (2012) 53.
23. H.W. Liang, Q.F. Guan, L.F. Chen, Z. Zhu, W.J. Zhang and S.H. Yu, *Angew. Chem. Int. Ed.* 51 (2012) 5101.
24. L. Fu, K. Tang, C.C. Chen, L. Liu, X. Guo, Y. Yu and J. Maier, *Nanoscale* 5 (2013) 11568;
25. J.H. Kim, K.H. Lee, L.J. Overzet and G.S. Lee, *Nano Lett.* 11 (2011) 2611.
26. Y. Chen, Z. Lu, L. Zhou, Y. W. Mai and H. Huang, *Energy Environ. Sci.* 5 (2012) 7898.
27. G. Singh, R. Thomas, A. Kumar, R.S. Katiyar and A. Manivannan, *J. Electrochem. Soc.* 159 (2012) A470.
28. D. Shin, C. Wolverton, J.R. Croy, M. Balasubramanian, S.H. Kang, C.M. L. Rivera and M. M. Thackeray, *J. Electrochem. Soc.* 159 (2012) A121.
29. C. S. Johnson, N. Li, C. Lefief, J. T. Vaughey and M. M. Thackeray, *Chem. Mater.* 20 (2008)

6095.
30. X. Zhang, S. Tang and Y. Du, *J. Phys. Chem. C* 115 (2011) 2644.
31. X. Zhang, S. Tang and Y. Du, *Phys. Lett. A* 375 (2011) 3196.
32. H. Yu, H. Kim, Y. Wang, P. He, D. Asakura, Y. Nakamura and H.S. Zhou, *Phys. Chem. Chem. Phys.* 14 (2012) 6584.
33. A.R. Armstrong, M. Holzapfel, P. Nova, C.S. Johnson, S.H. Kang, M.M. Thackeray and P.G. Bruce, *J. Am. Chem. Soc.* 128 (2006) 8694.
34. N. Yabuuchi, K. Yoshii, S.T. Myung, I. Nakai and S. Komaba, *J. Am. Chem. Soc.* 133 (2011) 4404.
35. J. Lim, J. Moon, J. Gim, S. Kim, K. Kim, J. Song, J. Kang, W.B. Im and J. Kim, *J. Mater. Chem.* 22 (2012) 11772.
36. C. Yu, G. Li, X. Guan, J. Zheng and L. Li, *Electrochim. Acta* 61 (2012) 216.
37. J.R. Croy, D. Kim, M. Balasubramanian, K. Gallagher, S. H. Kang and M.M. Thackeray, *J. Electrochem. Soc.* 159 (2012) A781.
38. F. Wang, S. Xiao, Y. Hou, C. Hu, L. Liu and Y. Wu, *RSC Adv.* 3 (2013) 13059.
39. K. Kubota, T. Kaneko, M. Hirayama, M. Yonemura, Y. Imanari, K. Nakane and R. Kanno, *J. Power Sources* 216 (2012) 249.
40. J. Zheng, M. Gu, J. Xiao, P. Zuo, C. Wang and J. G. Zhang, *Nano Lett.* 13 (2013) 3824.
41. Y.K. Sun, M.J. Lee, C.S. Yoon, J. Hassoun, K. Amine and B. Scrosati, *Adv. Mater.* 24 (2012) 1192.
42. Y. Wu, A. Vadivel Murugan and A. Manthiram, *J. Electrochem. Soc.* 155 (2008) A635.
43. C. Li, H.P. Zhang, L.J. Fu, H. Liu, Y.P. Wu, E. Rahm, R. Holze and H. Q. Wu, *Electrochim. Acta* 51 (2006) 3872 and references therein.